Active Loop Extrusion guides DNA-Protein Condensation

Ryota Takaki,[1] Yahor Savich,[1,2,3] Jan Brugués,[1,2,3,4,*] and Frank Jülicher[1,3,4,†]

[1] *Max Planck Institute for the Physics of Complex Systems*
[2] *Max Planck Institute of Molecular Cell Biology and Genetics (MPI-CBG), Dresden, Germany*
[3] *Center for Systems Biology Dresden, Dresden, Germany*
[4] *Cluster of Excellence Physics of Life, TU Dresden, Dresden, Germany*

(Dated: July 3, 2024)

The spatial organization of DNA involves DNA loop extrusion and the formation of protein-DNA condensates. While the significance of each process is increasingly recognized, their interplay remains unexplored. Using molecular dynamics simulation and theory we investigate this interplay. Our findings reveal that loop extrusion can enhance the dynamics of condensation and promotes coalescence and ripening of condensates. Further, the DNA loop enables condensate formation under DNA tension and position condensates. The concurrent presence of loop extrusion and condensate formation results in the formation of distinct domains similar to TADs, an outcome not achieved by either process alone.

How cells read and process genomic information represents a fundamental question that is not fully understood. This process involves physical interactions between DNA and proteins that transduce sequence information on DNA to express genes and to organize chromatin. Loop extrusion by structural maintenance of chromosomes (SMC) complexes have been identified as a primary candidate of genome organisation and regulation [1–5]. Loop extrusion has been studied through both *in vitro* experiments [6–17] and theoretical approaches [18–25]. DNA loops are involved in the formation of Topologically Associating Domains (TADs) in chromatin. TAD boundaries are determined by the position of CCCTC-binding factor (CTCF) molecules on the DNA [4, 26–31]. Another key process involved in chromatin organization is the formation of biological condensates, a process similar to phase separation [32–40]. Such condensates have been suggested, for example, to play a role in bringing promoters and enhancers into physical proximity [41]. Indeed condensates have been shown to exert capillary forces which could be involved in such processes [42]. These capillary forces are of similar magnitude as forces exerted by SMC molecules during loop extrusion [42]. This raises the question of how loop extrusion and condensate formation synergize to organize chromatin.

In this letter, we use simulation and theory to explore the interplay between loop extrusion and protein condensation in the spacial organization of DNA. We report that DNA loops play a pivotal role in nucleating and positioning protein-DNA co-condensates. The DNA loops not only facilitate the formation of co-condensates but also contribute to their stability under mechanical tension along DNA. We further discuss how loop extrusion and condensation contribute to the emergence of domains in chromatin contact maps, which characterize the DNA spatial organization.

* jan.brugues@tu-dresden.de
† julicher@pks.mpg.de

Here we consider a configuration often used in biophysical studies of DNA, where a single DNA molecule is attached at both ends to a surface [7, 42] (Fig.1). We perform Langevin dynamics simulations that incorporate three distinct types of particle representing DNA segments, proteins, and SMC molecules. These particles interact according to Lennard-Jones potentials as well as FENE potentials along the DNA contour [43]. DNA-Protein and Protein-Protein interactions are attractive while the interaction among DNA segments is repulsive. DNA segments are coarse-grained by particles with 10 nm diameter, and all three particle types have the same diameter. SMC molecules can bind to the DNA strand in the region indicated in blue in Fig.1. Upon binding of an SMC molecule to a DNA segment, a two-sided loop extrusion process is initiated. The loop extrusion process terminates when the extruded DNA reaches a boundary of the blue region, mimicking the role of CTCF molecules [26, 44]. We start our simulation from randomized initial positions of proteins and DNA segments, with DNA ends fixed at a prescribed distance $L_{\rm end}$ μm. The contour length of DNA is set to $L_c = 16.5$ μm, corresponding to λ-DNA [42]. See Supplementary Information (SI) for simulation details.

We first focus on the dynamics of condensate growth. Similar to conventional droplet kinetics, DNA-protein condensates grow through coalescence and Ostwald ripening when multiple condensates exist. Fig.2a displays the size S of the largest droplet as a function of simulation time t, averaged over three simulation trajectories. The size S is defined as the number of DNA and protein particles contained in the condensate (section IV.A in the SI). Step-wise increases of $S(t)$ indicate coalescence events, while gradual growth corresponds to ripening. We compare simulations without loop extrusion (Fig.2a, left) to simulations with loop extrusion (Fig.2a, right) for different $L_{\rm end}$. This comparison reveals that loop extrusion accelerates ripening but also enhances coalescence.

To provide further insight into the condensate growth dynamics, we count the number of events where condensates disappear either by coalescence or by Ostwald

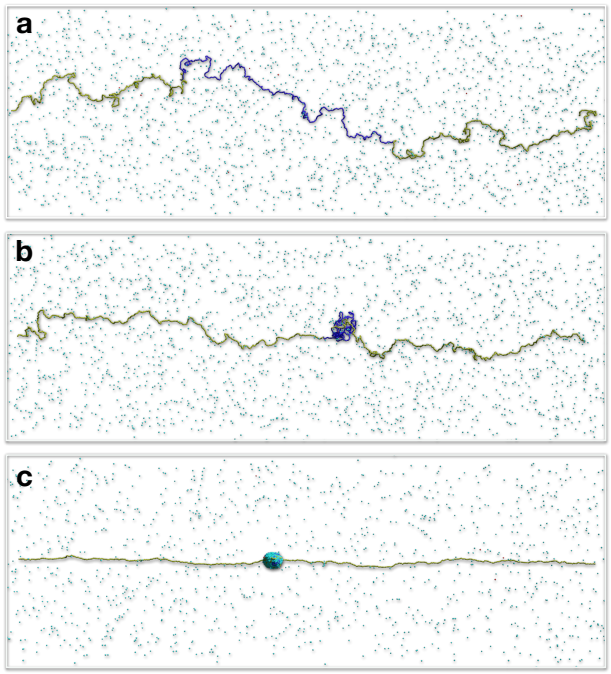

FIG. 1. (a) Initial configuration of the simulation with yellow and blue DNA particles indicating the DNA strand and SMC binding sites on DNA, respectively. Light blue particles represent proteins, and red particles SMC molecules. (b) Example of a DNA loop created by an SMC molecule. (c) Example of a Protein-DNA co-condensate. (a)-(c) are independent simulations for $L_{\rm end} = 6$ μm.

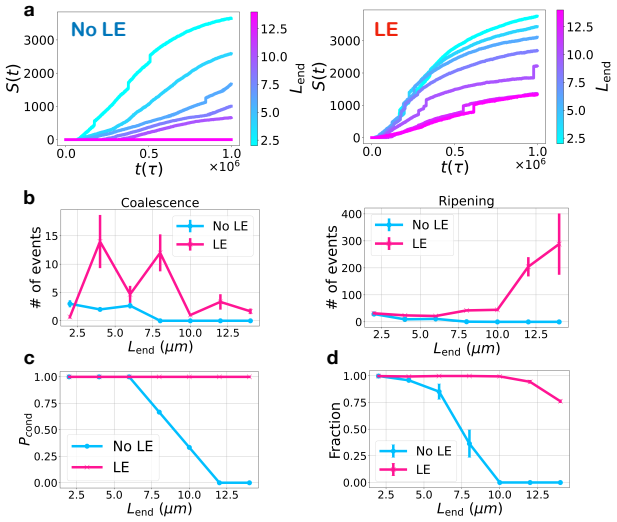

FIG. 2. (a) Size of the largest condensates $S(t)$ as a function of time t. Here τ is the unit-time in our simulation (SI). The color bars represent the DNA end-to-end distance, $L_{\rm end}$. Results without loop extrusion (No LE) and with loop extrusion (LE) are shown. (b) Number of condensate disappearance events due to droplet coalescence (left) or disassembly during ripening (right). Lines represent scenarios without loop extrusion (blue) and with loop extrusion (red). (c) Probability of condensate presence in the final frame of the simulation. (d) Fraction of SMC-binding DNA segments (blue in Fig.1) within the condensate. Error bars indicate the standard error across three simulations with same parameter values.

ripening, see Fig.2b. We find a systematic increase of condensate coalescence events in the presence of loop extrusion as compared to the absence of loop extrusion. Furthermore we observe that droplet disappearance by ripening is strongly enhanced for large $L_{\rm end}$. The enhancement of Ostwalt ripening by loop extrusion can be understood as follows: condensates outside the loop are subjected to the tension of the polymer and therefore disfavored as compared to the condensate inside the loop which is not subject to tension (section II in the SI).

We next calculated the probability of condensate formation ($P_{\rm cond}$), defined as the probability of condensate formation in the final frame of our simulation trajectories (Fig. 2c). For short $L_{\rm end}$, a condensate is present irrespective of whether a loop was extruded. For larger $L_{\rm end}$ the probability to find a condensate drops and eventually vanishes if no loop is extruded, similar to previous results [42]. Interestingly, loop extrusion enables condensate formation even at large $L_{\rm end}$. Loop extrusion can also position condensates. In fact, in our simulations, condensates are often found where the loop is formed. To quantify this co-localization, we compute in Fig.2d the fraction of SMC-binding DNA segments (blue in Fig.1) within the condensate. With loop extrusion, these segments are largely included inside the condensate, even for larger values of $L_{\rm end}$. In contrast, without loop extrusion, this fraction decreases with increasing $L_{\rm end}$.

The positioning of condensates by loop extrusion can be discussed by considering three possible scenarios. In scenario (a), the DNA loop is located outside of the condensate (Fig.3a). In the scenario (b), the condensate is located at the DNA loop and only the DNA loop is inside the condensate (Fig.3b). Finally in scenario (c) the DNA loop is inside the condensate together with additional DNA segments of length δ (Fig.3c). Our simulations suggest that condensation within the DNA loop is not affected by mechanical tension. Therefore condensates form reliably in the scenario (b) and (c) containing the loop. To understand the effect of DNA loop on the formation of condensates, we use a simple model of co-condensation [42]. In this model, the free energy of the configuration is the sum, $F = F_d + F_p$, where

$$F_d(L_d) = -v\alpha L_d + \gamma 4\pi \left(\frac{3\alpha}{4\pi}\right)^{2/3} L_d^{2/3}, \qquad (1)$$

is the free energy of the condensate and

$$F_p(L_d, L_{\rm end}, L_c) = \frac{k_B T L_{\rm end}^2}{4 l_p}\left(\frac{1}{L_c - L_d - L_{\rm end}} + \frac{2}{L_c - L_d}\right) \qquad (2)$$

is the free energy of the non-condensed DNA. Here L_d is the length of the DNA segments inside the condensate, k_B is the Boltzmann constant, T represents the

temperature, and l_p is the persistence length of DNA. The parameters α, γ, and v are the inverse of the DNA packing density, surface tension of the condensate, and condensation free energy per volume, respectively [42]. Below we use parameters values obtained for forkhead box protein A1 [42]: $\alpha = 0.04\ \mu\text{m}^2$, $\gamma = 0.04\ \text{pN}\,\mu\text{m}^{-1}$, $v = 2.6\ \text{pN}\,\mu\text{m}^{-2}$ and $l_p = 50$ nm.

We first consider scenario (a) (Fig.3a). In this case the condensate is located outside the DNA loop of length L_A. We define the energy difference $\Delta F_a = F_d(L_d) + F_p(L_d, L_{\text{end}}, L_c - L_A) - F_p(0, L_{\text{end}}, L_c - L_A)$ as the difference of the free energy before and after condensate formation, where we have taken into account that the DNA contour length L_c is effectively reduced by the loop length L_A. The stable condensate size is then obtained by minimizing ΔF_a with respect to L_d.

In scenario (b), the condensate contains the DNA length $L_d = L_A$ and the free energy change due to condensate formation is simply given by $\Delta F_b = F_d(L_A)$. Correspondingly, in scenario (c), we define $\Delta F_c = F_d(L_A + \delta) + F_p(L_A + \delta, L_{\text{end}}, L_c) - F_p(L_A, L_{\text{end}}, L_c)$. When $\delta = 0$, the DNA length inside the condensate equals to the loop length L_A, reducing this case to scenario (b).

We show ΔF_a in Fig.3d, as well as ΔF_b for $L_{\text{end}} = 5\ \mu$m. Increasing the loop length L_A shifts the minimum position of ΔF_a towards smaller values of L_d until the condensate vanishes via a first-order phase transition, similar to the one reported previously [42]. Fig.3d reveals that $\Delta F_b < \Delta F_a$, implying that a condensate will always form inside the loop, irrespective of the tension on the DNA. Thus, the DNA loop guides condensate formation. Fig.3e, shows the conditional probability of generating a condensate outside the loop (P_a) as a function of L_{end}. Increasing L_A shifts the curves for P_a towards smaller L_{end} values: the tension induced by the DNA loop narrows the range where condensation outside the loop is possible. However condensates in the loop are always favored ($P_b = 1$).

Fig.3f shows the free energy profile ΔF_c as a function of δ together with ΔF_b. This shows that for sufficiently large L_{end} the free energy is minimal for $\delta = 0$ and the condensate size is equal to the loop size. We call this loop limited condensate. As L_{end} is decreased below the critical value L^c_{end}, F_c exhibits a minimum at $\delta > 0$ corresponding to a condensate containing a DNA segment that is longer than the loop. In this regime the condensate is tension limited. At $L_{\text{end}} = L^c_{\text{end}}$ where δ vanishes, a continuous second order transition occurs. Fig.3g shows the phase diagram for condensates in the presence of a loop. In the blue region, $\delta = 0$ and condensates are loop limited. In the red region, $\delta > 0$ and condensates are tension limited. Both regions meet at a second order transition line.

We now discuss the effects of loops on DNA conformations inside the condensates. Both condensation and loop extrusion lead to a local accumulation of DNA segments, see Fig. 1. Such accumulation fosters contacts

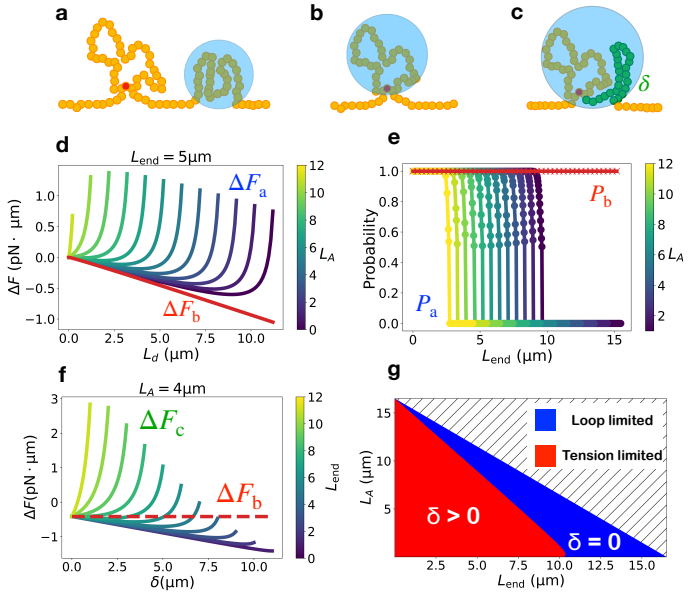

FIG. 3. (a)-(c) Schematic representations of three scenarios of protein-DNA co-condensation. Yellow, blue, and red circle indicates DNA segments, condensate, and SMC protein, respectively. (a) Condensate positioned outside the DNA loop. (b) Condensates at the DNA loop. (c) Condensate at the loop, including extra DNA length δ (green). (d) Free energy, ΔF_a, for scenario (a) compared to ΔF_b corresponding to (b), as a function of the length L_d within the condensate for different loop length L_A. (e) Probability P_a (P_b) of condensation formation for scenario (a) (scenario (b)) as a function of L_{end}. (f) Free energy ΔF_c for scenario (c) as a function of δ compared to ΔF_b for different L_{end}. (g) Phase diagram of condensation in the presence of DNA loop as a function of L_A and L_{end}. The loop limited regime (blue) and the tension limited regime (red) are indicated. The hatched region is physically inaccessible.

between DNA segments, even when they are at a distance along the sequence. The probabilities of such contacts are characterized by a contact map, a key tool to understand chromatin organization [45–49]. We determine contact maps for different end-to-end distance in our simulations. Fig.4 presents examples of contact maps with contact probability between two segments i and j, where i and j are the DNA particle indices of two DNA segments. In Fig. 4, contact maps are shown for DNA-protein co-condensation without loop extrusion (left column), for loop extrusion without condensation (middle column), and for both condensation and loop extrusion (right column), for different values of L_{end}. We find that if only condensation happens, contact maps show many but irregularly positioned disordered contacts for short L_{end}. These contacts disappear as L_{end} is increased and condensates dissolve. For only loop extrusion, contacts occur within the loop and are dominated by short-ranged contacts. When condensation and loop extrusion are combined, square patterns of contacts resembling TADs

emerge. These square patterns imply that contacts over longer distances along the chain are prominent.

To further characterise the structures generated by condensation and loop extrusion, we consider the polymeric configuration of loops and condensates. Fig.5a shows example configurations obtained in simulations: a DNA loop without condensation (left) and a DNA loop within a condensate (right). This reveals a coil-like structure of the DNA loop and a densely packed DNA within the condensate. Fig.5b shows, the radius of gyration (R_g) of the DNA loop as a function of loop length, exhibiting a scaling behavior with an exponent $\nu = 0.54$, similar to the Flory exponent $\nu = 3/5$ of a polymer in a good solvent [43]. In contrast, R_g of the DNA inside a condensate exhibits different scaling behavior with $\nu = 0.36$, which is close to the exponent $\nu = 1/3$ of a collapsed polymer in a poor solvent [43].

Using these results, we can explain the difference between the contact maps shown in Fig.4. In the absence of condensation, the looped polymer behaves as a random coil favoring short range contacts. Indeed, the contact probability decreases for increasing distance along the polymer, giving rise to the short ranged contact maps shown in Fig.4, middle. For a loop inside the condensate, the contact probability remains high, giving rise to the longer ranged contact map. We use a simple argument for the scaling of the contact probability $P \sim s^{-\kappa}$ as a function of the DNA length s between the contacts points. Assuming a probability of contacts proportional to the squared density, we have

$$P(s) \sim \left(\frac{s}{R_g^3}\right)^2 \sim s^{-2(3\nu-1)}. \qquad (3)$$

The Flory exponent of $\nu = 3/5$ for a good solvent implies $\kappa = 8/5$ while for a poor solvent $\nu = 1/3$ leads to $\kappa = 0$.

We tested this scaling argument in our simulation. Fig.5c (top) shows $P(s)$ for a loop without condensate. We find $\kappa \simeq 1.21$, which is in good agreement with the estimate $\kappa = 1.24$ using $\kappa = 6\nu - 2$ with $\nu = 0.54$ (Fig.5b, top). For loop extrusion with condensation, we obtained $\kappa \simeq 0.63$ (Fig.5c, bottom). This is longer ranged as compared to the case without condensate, but deviates from the estimate $\kappa = 0.16$ using $\nu = 0.36$ (Fig.5b, bottom). This difference may stem from finite-size and finite-time effects in our simulations. However, the change of the exponents for loops with ($\kappa = 0.63$) and without condensation ($\kappa = 1.21$) is significant, and highlights the longer range contacts in a condensed DNA loop.

In summary, we investigated the interplay between DNA loop extrusion and DNA-protein co-condensation. We found that loop extrusion stabilises DNA-protein co-condensation under tension and positions the condensate on DNA. We identified a regime of loop limited condensates, where condensates size is set by the DNA loop size. Our work shows that by combining loop extrusion and condensation, a DNA organization with the characteristics of TADs naturally emerges. In the absence of the condensation, the resulting contact maps remain short ranged. The condensation facilitates the close contacts of distant DNA segments within the TAD. Our work underscores chromatin organization in the nucleus may emerge from the interplay between loop extrusion and protein-DNA co-condensation.

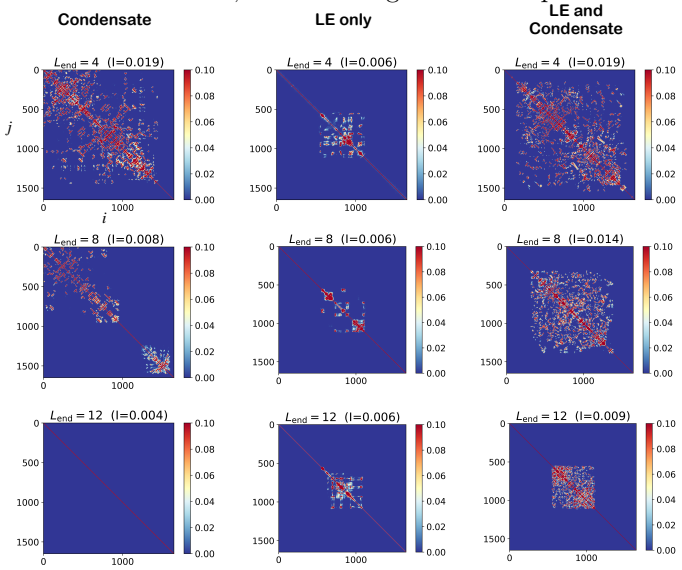

FIG. 4. Contact maps obtained in simulations for only condensation (left), only loop extrusion (middle), and both loop extrusion and condensation (right) as a function of DNA particle indices i and j. Contact maps are presented for $L_{\rm end} = 4, 8, 12$ μm (top to bottom). The contact probability between particle i and j is shown as a color code. The fraction I of contacts, defined as the sum of the all contact probabilities normalized by the total number of pairs (1650^2), is given.

[1] K. Nasmyth and C. H. Haering, Cohesin: its roles and mechanisms, Annual review of genetics **43**, 525 (2009).
[2] E. Kim, R. Barth, and C. Dekker, Looping the genome with smc complexes, Annual Review of Biochemistry **92** (2023).
[3] I. F. Davidson and J.-M. Peters, Genome folding through loop extrusion by smc complexes, Nature reviews Molecular cell biology **22**, 445 (2021).
[4] S. Yatskevich, J. Rhodes, and K. Nasmyth, Organization of chromosomal dna by smc complexes, Annual review of genetics **53**, 445 (2019).
[5] C. Hoencamp and B. D. Rowland, Genome control by smc complexes, Nature Reviews Molecular Cell Biology , 1 (2023).

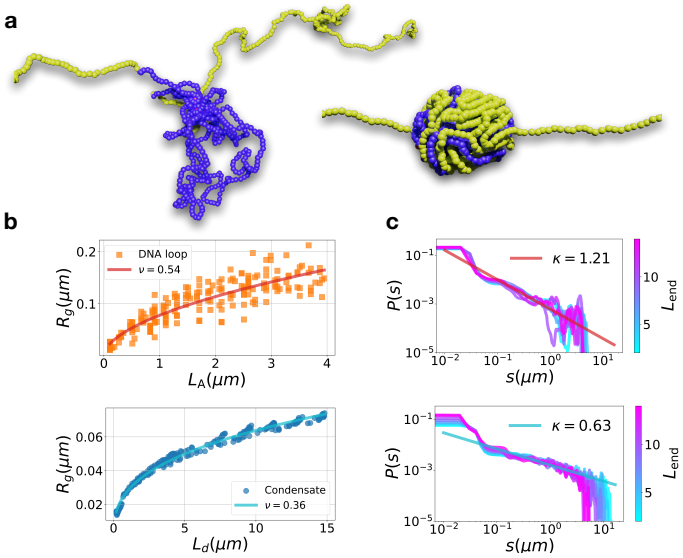

FIG. 5. (a) Representative snapshots showing a DNA loop without condensation (left) and a DNA-Protein condensate containing the DNA loop (right). Yellow and blue particles indicate the DNA strand and SMC binding site on DNA, respectively. Protein particles are not shown to emphasize the DNA structure. $L_{\rm end} = 6\ \mu m$. (b) Radius of gyration R_g of DNA loops without condensation as a function loop length L_A (top, $\nu \simeq 0.54$) and of DNA within a condensate as a function of condensed DNA length L_d (bottom, $\nu \simeq 0.36$). The data is fit using $R_g \sim L^{\nu}$ (solid lines). (c) Probability of contact, P, as a function of the DNA length between contacts, s, for different $L_{\rm end}$ for loop extrusion without condensation (top, $\kappa = 1.21$) and for loop extrusion with condensation (bottom, $\kappa = 0.63$). The data is fit using $P \sim s^{-\kappa}$ (solid lines). The reported values of κ are the mean value of the exponents for different $L_{\rm end}$ fit in the range $5 \cdot 10^{-2}\ \mu m < s < 3\ \mu m$.

[6] T. Terakawa, S. Bisht, J. M. Eeftens, C. Dekker, C. H. Haering, and E. C. Greene, The condensin complex is a mechanochemical motor that translocates along dna, Science **358**, 672 (2017).

[7] M. Ganji, I. A. Shaltiel, S. Bisht, E. Kim, A. Kalichava, C. H. Haering, and C. Dekker, Real-time imaging of dna loop extrusion by condensin, Science **360**, 102 (2018).

[8] S. Golfier, T. Quail, H. Kimura, and J. Brugués, Cohesin and condensin extrude dna loops in a cell cycle-dependent manner, Elife **9**, e53885 (2020).

[9] E. Kim, A. M. Gonzalez, B. Pradhan, J. van der Torre, and C. Dekker, Condensin-driven loop extrusion on supercoiled dna, Nature Structural & Molecular Biology **29**, 719 (2022).

[10] E. Kim, J. Kerssemakers, I. Shaltiel, C. Haering, and C. Dekker, Dna-loop extruding condensin complexes can traverse one another, Biophysical Journal **118**, 380a (2020).

[11] B. Pradhan, T. Kanno, M. Umeda Igarashi, M. S. Loke, M. D. Baaske, J. S. K. Wong, K. Jeppsson, C. Björkegren, and E. Kim, The smc5/6 complex is a dna loop-extruding motor, Nature , 1 (2023).

[12] I. F. Davidson, B. Bauer, D. Goetz, W. Tang, G. Wutz, and J.-M. Peters, Dna loop extrusion by human cohesin, Science **366**, 1338 (2019).

[13] Y. Kim, Z. Shi, H. Zhang, I. J. Finkelstein, and H. Yu, Human cohesin compacts dna by loop extrusion, Science **366**, 1345 (2019).

[14] J.-K. Ryu, S.-H. Rah, R. Janissen, J. W. Kerssemakers, A. Bonato, D. Michieletto, and C. Dekker, Condensin extrudes dna loops in steps up to hundreds of base pairs that are generated by atp binding events, Nucleic acids research **50**, 820 (2022).

[15] B. Pradhan, R. Barth, E. Kim, I. F. Davidson, B. Bauer, T. van Laar, W. Yang, J.-K. Ryu, J. van der Torre, J.-M. Peters, *et al.*, Smc complexes can traverse physical roadblocks bigger than their ring size, Cell reports **41** (2022).

[16] J.-K. Ryu, A. J. Katan, E. O. van der Sluis, T. Wisse, R. de Groot, C. H. Haering, and C. Dekker, The condensin holocomplex cycles dynamically between open and collapsed states, Nature structural & molecular biology **27**, 1134 (2020).

[17] G. Shi, L. Liu, C. Hyeon, and D. Thirumalai, Interphase human chromosome exhibits out of equilibrium glassy dynamics, Nature communications **9**, 3161 (2018).

[18] R. Takaki, A. Dey, G. Shi, and D. Thirumalai, Theory and simulations of condensin mediated loop extrusion in dna, Nature Communications **12**, 5865 (2021).

[19] E. J. Banigan and L. A. Mirny, Limits of chromosome compaction by loop-extruding motors, Physical Review X **9**, 031007 (2019).

[20] E. J. Banigan and L. A. Mirny, Loop extrusion: theory meets single-molecule experiments, Current opinion in cell biology **64**, 124 (2020).

[21] E. J. Banigan and L. A. Mirny, The interplay between asymmetric and symmetric dna loop extrusion, Elife **9**, e63528 (2020).

[22] B. Chan and M. Rubinstein, Theory of chromatin organization maintained by active loop extrusion, Proceedings of the National Academy of Sciences **120**, e2222078120 (2023).

[23] J. F. Marko, P. De Los Rios, A. Barducci, and S. Gruber, Dna-segment-capture model for loop extrusion by structural maintenance of chromosome (smc) protein complexes, Nucleic acids research **47**, 6956 (2019).

[24] A. Bonato and D. Michieletto, Three-dimensional loop extrusion, Biophysical Journal **120**, 5544 (2021).

[25] B. Chan and M. Rubinstein, Activity-driven chromatin organization during interphase: compaction, segregation, and entanglement suppression, Proceedings of the National Academy of Sciences **121**, e2401494121 (2024).

[26] I. F. Davidson, R. Barth, M. Zaczek, J. van der Torre, W. Tang, K. Nagasaka, R. Janissen, J. Kerssemakers, G. Wutz, C. Dekker, *et al.*, Ctcf is a dna-tension-dependent barrier to cohesin-mediated loop extrusion, Nature , 1 (2023).

[27] D. Jeong, G. Shi, X. Li, and D. Thirumalai, Structural basis for the preservation of a subset of topologically associating domains in interphase chromosomes upon cohesin depletion, Elife **12**, RP88564 (2024).

[28] W. Schwarzer, N. Abdennur, A. Goloborodko, A. Pekowska, G. Fudenberg, Y. Loe-Mie, N. A. Fonseca, W. Huber, C. H. Haering, L. Mirny, *et al.*, Two independent modes of chromatin organization revealed by cohesin removal, Nature **551**, 51 (2017).

[29] G. Fudenberg, M. Imakaev, C. Lu, A. Goloborodko, N. Abdennur, and L. A. Mirny, Formation of chromo-

somal domains by loop extrusion, Cell reports **15**, 2038 (2016).

[30] E. J. Banigan, W. Tang, A. A. van den Berg, R. R. Stocsits, G. Wutz, H. B. Brandão, G. A. Busslinger, J.-M. Peters, and L. A. Mirny, Transcription shapes 3d chromatin organization by interacting with loop extrusion, Proceedings of the National Academy of Sciences **120**, e2210480120 (2023).

[31] A. Dey, G. Shi, R. Takaki, and D. Thirumalai, Structural changes in chromosomes driven by multiple condensin motors during mitosis, Cell Reports **42** (2023).

[32] A. A. Hyman, C. A. Weber, and F. Jülicher, Liquid-liquid phase separation in biology, Annual review of cell and developmental biology **30**, 39 (2014).

[33] K. Rippe, Liquid–liquid phase separation in chromatin, Cold Spring Harbor perspectives in biology **14**, a040683 (2022).

[34] J. T. King and A. Shakya, Phase separation of dna: From past to present, Biophysical Journal **120**, 1139 (2021).

[35] K. Shrinivas, B. R. Sabari, E. L. Coffey, I. A. Klein, A. Boija, A. V. Zamudio, J. Schuijers, N. M. Hannett, P. A. Sharp, R. A. Young, and A. K. Chakraborty, Enhancer features that drive formation of transcriptional condensates, Molecular Cell **75**, 549 (2019).

[36] M.-T. Wei, Y.-C. Chang, S. F. Shimobayashi, Y. Shin, A. R. Strom, and C. P. Brangwynne, Nucleated transcriptional condensates amplify gene expression, Nature cell biology **22**, 1187 (2020).

[37] J. E. Henninger, O. Oksuz, K. Shrinivas, I. Sagi, G. LeRoy, M. M. Zheng, J. O. Andrews, A. V. Zamudio, C. Lazaris, N. M. Hannett, *et al.*, Rna-mediated feedback control of transcriptional condensates, Cell **184**, 207 (2021).

[38] J. A. Morin, S. Wittmann, S. Choubey, A. Klosin, S. Golfier, A. A. Hyman, F. Jülicher, and S. W. Grill, Sequence-dependent surface condensation of a pioneer transcription factor on dna, Nature Physics **18**, 271 (2022).

[39] R. Renger, J. A. Morin, R. Lemaitre, M. Ruer-Gruss, F. Jülicher, A. Hermann, and S. W. Grill, Co-condensation of proteins with single-and double-stranded dna, Proceedings of the National Academy of Sciences **119**, e2107871119 (2022).

[40] J.-U. Sommer, H. Merlitz, and H. Schiessel, Polymer-assisted condensation: A mechanism for heterochromatin formation and epigenetic memory, Macromolecules **55**, 4841 (2022).

[41] A. Panigrahi and B. W. O'Malley, Mechanisms of enhancer action: the known and the unknown, Genome biology **22**, 108 (2021).

[42] T. Quail, S. Golfier, M. Elsner, K. Ishihara, V. Murugesan, R. Renger, F. Jülicher, and J. Brugués, Force generation by protein–dna co-condensation, Nature Physics **17**, 1007 (2021).

[43] M. Rubinsten, *Polymer physics* (United States of America, 2003).

[44] M. Gabriele, H. B. Brandão, S. Grosse-Holz, A. Jha, G. M. Dailey, C. Cattoglio, T.-H. S. Hsieh, L. Mirny, C. Zechner, and A. S. Hansen, Dynamics of ctcf-and cohesin-mediated chromatin looping revealed by live-cell imaging, Science **376**, 496 (2022).

[45] E. Lieberman-Aiden, N. L. Van Berkum, L. Williams, M. Imakaev, T. Ragoczy, A. Telling, I. Amit, B. R. Lajoie, P. J. Sabo, M. O. Dorschner, *et al.*, Comprehensive mapping of long-range interactions reveals folding principles of the human genome, science **326**, 289 (2009).

[46] G. Shi and D. Thirumalai, Conformational heterogeneity in human interphase chromosome organization reconciles the fish and hi-c paradox, Nature communications **10**, 3894 (2019).

[47] G. Shi and D. Thirumalai, A maximum-entropy model to predict 3d structural ensembles of chromatin from pairwise distances with applications to interphase chromosomes and structural variants, Nature Communications **14**, 1150 (2023).

[48] G. Shi and D. Thirumalai, From hi-c contact map to three-dimensional organization of interphase human chromosomes, Physical Review X **11**, 011051 (2021).

[49] S. Shin, G. Shi, and D. Thirumalai, From effective interactions extracted using hi-c data to chromosome structures in conventional and inverted nuclei, PRX Life **1**, 013010 (2023).